

Intrinsic structure of the free liquid surface of an alkali metal

E. Chacón,¹ P. Tarazona,² and L. E. González³

¹*Instituto de Ciencia de Materiales de Madrid, Consejo Superior de Investigaciones Científicas, Cantoblanco, E-28049 Madrid, Spain*

²*Departamento de Física Teórica de la Materia Condensada, and Instituto Nicolás Cabrera, Universidad Autónoma de Madrid, E-28049 Madrid, Spain*

³*Departamento de Física Teórica, Universidad de Valladolid, 47011 Valladolid, Spain*

(Received 21 July 2006; published 4 December 2006)

An operational procedure to obtain the intrinsic properties of free liquid surfaces, and which had been previously applied to computer simulations of dielectric liquid models, is used here to sample the intrinsic surface properties of liquid lithium, sodium, and potassium, with an *ab initio* orbital free description of the electrons. When properly scaled, the intrinsic profiles of the three alkali fluids turn to be virtually identical. As in simple fluid models these intrinsic density profiles show a strong layering structure, similar to that of the bulk liquid pair distribution function, but with specific surface aspects like the density of the first liquid layer, and the interlayering spacing. The capillary wave fluctuations of the surface partially damp the intrinsic layering and produce density profiles which depend strongly on the transverse sampled area, but which still show an oscillating structure. The assumptions of the capillary wave theory, which is used in the interpretation of x-ray reflectivity data, may be directly checked, and a direct comparison with the experimental data presented, with very good agreement between our results and the measured electronic surface structure factor for potassium.

DOI: [10.1103/PhysRevB.74.224201](https://doi.org/10.1103/PhysRevB.74.224201)

PACS number(s): 61.25.Mv, 68.03.Hj, 68.03.Kn

I. INTRODUCTION

The structure of the liquid-vapor interface is a subject of renewed experimental and computational interest, with emphasis on the possible existence of liquid surface layers. Free liquid surfaces present an important challenge for experimentalists, since the capillary waves (CW) surface thermal fluctuations produce a damping of the surface structure, so that the mean density profile $\rho(z, L_x)$, sampled over a transverse area $A \equiv L_x^2$, becomes more blurred for increasing L_x . However, starting in 1995, the increased accuracy of the x-ray reflectivity techniques has reduced the linear transverse sampling size to $L_x \sim 10^3$ Å, and it has allowed one to obtain clear evidence of the existence of atomic surface layering in a number of liquid metals¹⁻⁴ and alloys.⁵ Only very recently, has similar evidence been obtained of molecular layering at the surface of a dielectric liquid,⁶ which shares with the liquid metals Hg and Ga a very low ratio between the triple and the critical temperatures. The low melting temperature provides stability for the cold liquid phases, with very stiff surfaces and small CW amplitudes, and this seems to be the essential requirement for the observation of surface layering density oscillations.⁷ The smaller transverse size of computer simulations, typically with L_x between 5 and 20 times the molecular diameter σ , has allowed the direct observation of surface layering in several simple fluid models with $T_l/T_c \leq 0.3$,⁷⁻⁹ and the recent computer simulations for the free liquid surface of simple metals, with an orbital-free *ab initio* description of the conduction electrons,¹⁰⁻¹² offers the first opportunity for quantitative comparison between experimental evidence of surface layering of liquid potassium⁴ and a realistic computer simulation for the same system with explicit knowledge of the transverse sampling size, $L_x \approx 40$ Å. Notice that any previous theoretical treatment for the surface of liquid metals had not taken into account the long wave

spectrum of CW fluctuations, and the induced L_x dependence of the mean density profiles. The methods based on classical density functional treatments (CDFT),¹³ do not have any dependence on L_x at all. The mixed approach¹⁴ with Monte Carlo simulations for the ions on the effective self-consistent potential created by the conduction band electrons, use a reference *jellium* system with density $\rho_{\text{jell}}(z)$, i.e., without any instantaneous structure on the transverse plane, over $\mathbf{R} \equiv (x, y)$; hence that approach would fail to reproduce a long wavelength spectrum of CW fluctuations. Therefore the ionic density profiles obtained with these methods have to be interpreted as $\rho(z, L_x^{\text{eff}})$, associated to an unknown effective transverse sampling size L_x^{eff} . For density functional treatments of simple fluid models there is an estimation¹⁵ of $L_x^{\text{eff}} \approx 8-14\sigma$, with some unavoidable ambiguity in the interpretation. For the much more complex theoretical treatment of liquid metals we do not have any quantitative estimation for L_x^{eff} , although we may expect that L_x^{eff} is also of the order of ten atomic diameters, since the alkali mean ionic density profiles obtained by Rice *et al.*¹⁴ are very similar to those obtained by Gonzalez *et al.*¹⁰

The experimental x-ray reflectivity data are interpreted within the capillary wave theory (CWT),¹⁶ which predicts the dependence of the density profiles on the transverse sampling size L_x . The mean density profile $\rho(z, L_x)$ is the convolution of an *intrinsic profile*, $\tilde{\rho}(z, q_u)$, with a CW Gaussian distribution of mean squared width $\Delta_{\text{CWT}}(L_x, q_u)$. The intrinsic density profile may be regarded as the result of a transverse sampling at molecular scale, with an effective linear size $L_x^l = 2\pi/q_u$ on the range of the molecular diameter σ , and hence much smaller than the experimental resolution for x-ray reflectivity. The CWT also assumes that, for wave vectors between $2\pi/L_x$ and q_u , the CW spectrum may be described with the macroscopic surface tension γ , so that the squared Gaussian width of the CW amplitude distribution is

$\Delta_{\text{CWT}}(L_x, q_u) = kT / (2\pi\gamma) \log(L_x q_u / 2\pi)$. For monotonic shapes of the intrinsic density profile, the Gaussian convolution with the CW fluctuations is reflected on the increase of the interfacial width for the mean density profile $\rho(z, L_x)$. However, that weak logarithmic dependence of the density profile on L_x is often waived in the direct comparison of theoretical density functional results for $\rho(x)$, and computer simulation samplings $\rho(x, L_x)$ for simple liquids. Whenever $\tilde{\rho}(z, q_u)$ presents an oscillatory structure due to surface layering, the L_x dependence of the mean density profiles becomes much more important, since the Gaussian convolution damps the amplitude of the density oscillations with an exponential factor $L_x^{-\eta}$, with an exponent $\eta \approx 2\pi / (\beta\gamma\sigma^2)$. Therefore unless $\eta \ll 1$ a liquid surface would have very different mean density profiles $\rho(z, L_x)$ for different transverse sampling L_x , and any comparison between the experimental and theoretical observations of surface layering, or even between computer simulations with different values of L_x , should take this fact into account.

The interpretation of the experimental x-ray reflectivity data¹⁻⁴ is done in terms of the intrinsic profile associated to an empirical upper wave-vector cutoff $q_u = \pi/\sigma$, which is assumed to cover the full spectrum of CW fluctuations. The quantitative use of the CWT assumptions at such a sharp level of atomic resolution presents clear incertitudes, which have been recently explored with an *intrinsic sampling method* applied to computer simulations of simple¹⁷⁻¹⁹ and molecular²⁰ fluids. The method is based on the self-consistent identification of the *first liquid layer*, and in its use to define the *intrinsic surface*, $z = \xi(\mathbf{R})$, as the assumed instantaneous boundary between the two bulk coexisting phases, which is the basic concept of the CWT; the *intrinsic density profiles* reflect the distribution of the ions relative to the instantaneous intrinsic surface, so that the CW blurring effect is eliminated, and the dependence with the transverse sampling size disappears. The application of this intrinsic sampling method to the surfaces of simple fluids,^{17,18} and water,²⁰ has shown that surface layering, and hence the strong dependence of the mean profiles with L_x , are a generic property of liquid surfaces. The complete damping of the intrinsic layering, leading to monotonic mean profiles $\rho(z, L_x)$, would happen at different transverse sizes, depending on the value of the η exponent, ranging from $L_x \approx 3\sigma$ for the Lennard-Jones model, to some thousands of atomic diameters for Hg or Ga. The apparent qualitative difference between layered and smooth liquid surfaces reflects only the typical sampling size in experiments ($L_x \sim 10^3$ Å) and in computer simulations ($L_x \sim 10\sigma$).

In this paper we present the application of that *intrinsic sampling method* to the computer simulations of the free surface of liquid Li, Na, and K carried out by Gonzalez *et al.*¹⁰⁻¹² for the surface of several liquid metals, in order to discern any common behavior for alkali systems, and also to compare the results obtained for K with those extracted from the x-ray reflectivity measurements of Ref. 4. The opportunity of this first contact between the experimental observation of surface layering in liquid metals, and a realistic computer simulation for the same system, with well-characterized transverse sampling size, is taken to its sharper

resolution through the direct comparison of the intrinsic density profiles $\tilde{\rho}(z, q_u)$ obtained under accurately controlled values of the upper cutoff q_u , in the analysis of the computer simulation results. The empirically assumed level of roughness for the intrinsic surface, $q_u = \pi/\sigma$, and the validity of the effective CWT surface Hamiltonian used in the interpretation of the experimental data may be directly tested, to put this interpretation on a quantitatively firmer basis. In the next section we present the details of the simulation and the calculation of the electron-ion interactions, together with a discussion on the qualitative difference with the previous computer simulations of Rice and co-workers.¹⁴ In Sec. III we apply the intrinsic sampling method to extract the intrinsic density profiles of liquid surfaces for liquid Li, Na, and K. In Sec. IV the extracted intrinsic electronic density profile of liquid K is used to get the surface structure factor, which is compared with the experimental results obtained from x-ray reflectivity. We end with a general discussion on the structure of fluid interfaces and their view through the intrinsic sampling in computer simulations.

II. MODEL AND MOLECULAR DYNAMIC SIMULATION

A simple metal is treated as a set of N ions with valence Z , enclosed in a volume V and interacting with $N_e = NZ$ valence electrons through electron-ion pseudopotentials. The total potential energy of the system can be written, within of the Born Oppenheimer approximation, as the sum of the direct ion-ion Coulombic interaction and the ground state energy of the electronic system, $E_g[\rho_g(\mathbf{r})]$. The electronic properties are obtained through electronic density functional theory (EDFT), according to which the ground state electronic density, $\rho_g(\mathbf{r})$, minimizes an energy functional which is given as the sum of the kinetic energy of independent electrons, $T_s[\rho]$, the classical Hartree electrostatic energy, $E_H[\rho]$, the exchange correlation energy, $E_{xc}[\rho]$, for which we have adopted the local density approximation, and finally, the electron-ion interaction energy, $E_{\text{pseud}}[\rho]$, for which we have used local ionic pseudopotentials constructed within EDFT.²¹ In the Kohn-Sham (KS) version of the method,²² $T_s[\rho]$ is calculated exactly by using single particles orbitals, which requires a huge computational effort, limiting the samples size and the simulation times: in the particular case of liquid metal surfaces the maximum number of atoms that could be afforded within a KS-EDFT simulation is around 160 (Ref. 23). For that reason our simulations have been carried out using the orbital-free *ab initio* molecular dynamics (OFAIMD). This method uses an explicit approximation for the electron kinetic energy functional of the EDFT but otherwise correctly treats the forces on the ions. The approximation greatly simplifies the calculation allowing simulation of much larger samples for long times. An essential component of proposed kinetic energy functionals is the von Weizsäcker term,

$$T_w[\rho(\mathbf{r})] = \frac{1}{8} \int d\mathbf{r} \frac{|\nabla\rho(\mathbf{r})|^2}{\rho(\mathbf{r})}, \quad (1)$$

and the kinetic-energy functional is usually written as

TABLE I. Simulation parameters for the systems studied. E_c is the cutoff energy in the plane-wave expansion and t is the total time of the equilibrium simulation. Also shown is the position σ of the first peak of the bulk pair correlation function.

Metal	ρ (\AA^{-3})	T (K)	L_x (\AA)	E_c (Ry)	t (ps)	σ (\AA)
Li	0.0445	470	28.44	9.50	108.00	2.92
Na	0.0242	373	33.50	7.50	61.75	3.51
K	0.0127	343	44.99	5.25	125.50	4.26

$$T_s[\rho] = T_w[\rho(\mathbf{r})] + T_{nl}[\rho(\mathbf{r})], \quad (2)$$

where $T_{nl}[\rho]$ is of highly nonlocal nature. Many models following this scheme have been proposed.²⁴ In the present paper we have used a modification of the functional proposed by García-González *et al.*²⁵ that enables a rapid computation of T_{nl} through fast Fourier transforms and includes some appealing mathematical properties.²¹ Another key ingredient is the local pseudopotential $v_{ps}(\mathbf{r})$, describing the ion-electron interaction; it has been developed from first principles by fitting, within the same $T_s[\rho]$ functional, the displaced electronic density induced by an ion immersed in a metallic medium as obtained in a KS calculation.²¹ The combination of this local pseudopotential along with the previous $T_s[\rho]$ functional has provided an accurate description of several static and dynamic properties of bulk²¹ and surface¹⁰ metallic liquids.

OFAIMD simulations for the liquid surface in Li, Na, and K are presented for thermodynamic conditions near their respective triple points. We have considered slabs consisting of 2000 ions in a supercell with two free surfaces normal to the z axis. The dimensions of the slab were initially $L_x \times L_x \times 2L_x$, with a further 8 \AA of vacuum added above and below the slab. Given the ionic positions at time t , the electron density is expanded in plane waves and the energy functional minimized with respect to the plane-wave coefficients yielding the ground state electronic density, energy, and the forces on the ions, and finally the ionic positions and velocities are updated using Verlet's leap-frog algorithm. For all systems, equilibration lasted for 15 ps. The parameters of the simulations for the three elements are given in Table I.

The usual description of the liquid-vapor interface is through the mean density profile, defined as the statistical sampling over a transverse area $A=L_x^2$.

$$\rho(z, L_x) \equiv \left\langle \frac{1}{A} \sum_{i=1}^N \delta(z - z_i) \right\rangle. \quad (3)$$

In Fig. 1 we present the mean density profiles $\rho(z, A)$ for K, the results for Li and Na are very similar and have been shown in Refs. 10 and 12. As we can see the ionic density profiles exhibit a clear layering structure for about five layers into the bulk liquid. That means that the intrinsic profile has a layering structure and that the CW damping has not erased it completely because the value of η is relatively low. The total-electron mean density profiles are very similar to the ion profile because they are dominated by the localized and

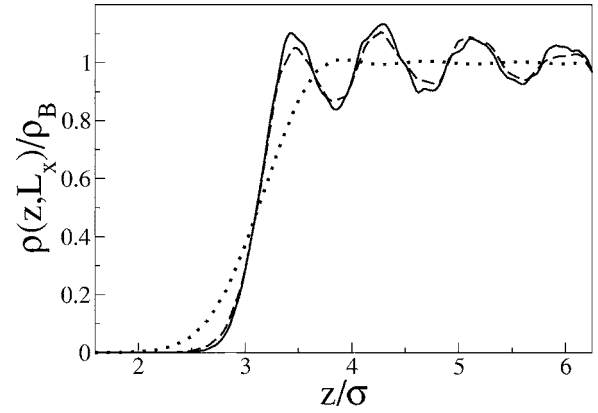


FIG. 1. Ionic (full line), total (core+valence) electron (dashed line), and valence electron (dotted line) mean density profiles $\rho(z, L_x)$ normal to the surface of K at $T/T_C=0.507$. The distance, z , is in units of the position of the first peak of the bulk pair correlation function.

more numerous core electrons. However, the valence electron-density profiles show a very weak surface layering, with much smaller amplitude and oscillating on the opposite phase of the ionic oscillations. A detailed discussion about these mean profiles has been carried out in Refs. 10–12. The goal of the present paper is the study of the intrinsic profiles.

It is important to mark the differences between the present OFAIMD simulations and previous treatments of the problem. In CDFT treatments of liquid metal surfaces,¹³ the grand potential free energy of the system is minimized with respect to the density profiles $\rho(z)$ and $\rho_{elec}(z)$, which represent the *mean* density distributions of ions and valence electrons. These profiles have no dependence on the transverse area, since the density functional approximations used to describe the free energy dependence on $\rho(z)$, and $\rho_{elec}(z)$, are based on perturbation theories, and they do not contain the specific long-range transverse surface correlations induced by the surface fluctuations. The mixed approach, with perturbation theory and computer simulations, developed by Rice and co-workers¹⁴ implies the use of a *jellium* reference system, with a density distribution $\rho_{jell}(z)$ fitted to the instantaneous distribution of the ions, but which (i) is smooth, i.e., does not have any oscillations, and (ii) is flat, i.e., does not follow any local roughness on the transverse plane. This later assumption is clearly reflected in the valence electron density profiles of Rice *et al.*, which have much stronger density oscillations than those in Fig. 1, since the CW effects on the valence electron are fully eliminated by the flat ionic *jellium*. However, within the transverse size of the MD simulations the suppression of the electron transverse surface fluctuations does not appear to have an important effect on the CW spectrum of the ions, since the mean ionic density profiles are very similar to both methods. Nevertheless, only with the fully self-consistent OFAIMD approach used here, we may expect that the L_x dependence of the density profiles follows the predictions of the CWT for large transverse size.

III. INTRINSIC SURFACE SAMPLING AND PROFILES

The CWT postulates that for each instantaneous molecular configuration of a liquid surface, we may find an intrinsic

surface $z=\xi(\mathbf{R})$, with $\mathbf{R}=(x,y)$, which represents the microscopic frontier between the liquid and vapor phases. Although the theory does not specify the definition for $\xi(\mathbf{R})$, it assumes that it may be used to obtain the intrinsic density profile, defined as the average over all configurations of the instantaneous microscopic density referred to the intrinsic surface $\xi(\mathbf{R},q_u)$:

$$\bar{\rho}(z,q_u) = \left\langle \frac{1}{A} \sum_{i=1}^N \delta[z - z_i + \xi(\mathbf{R}_i, q_u)] \right\rangle. \quad (4)$$

Usually the intrinsic surface is described through its Fourier components:

$$\xi(\mathbf{R}, q_u) = \sum_{|\mathbf{q}|=q_l}^{q_u} \hat{\xi}_{\mathbf{q}} e^{i\mathbf{q}\cdot\mathbf{R}}, \quad (5)$$

with the sum over transverse wave vectors, $\mathbf{q} = 2\pi(n_x, n_y)/L_x$ and $n_x, n_y = 0, \pm 1, \pm 2, \dots$, to include the periodic boundary conditions on the transverse direction, in a computer simulation box. Note that these transverse wave vectors are specific to the simulation setup, and in particular the smallest wave vector, and consequently the lower limit in the CW spectrum, is $q_l = 2\pi/L_x$. We use here an operational definition of the instantaneous intrinsic surface which may be carried out automatically for samplings along computer simulations. A detailed account of the procedure to get $\xi(\mathbf{R}, q_u)$ has been presented in Refs 17 and 18, and in Ref. 19 the slight modification of the original procedure used in the present work. The *maximum* level of resolution for the intrinsic surface, $\xi(\mathbf{R}, q_m)$, is taken here with $q_m = 9q_l \approx 1.8\pi/\sigma$. That intrinsic surface is defined to have the minimum possible area, but going exactly through all the ions selected to represent the *first liquid layer*. To choose the ions in that layer, for each configuration of the liquid slab, we first use a percolation analysis to eliminate any ion with less than three neighbors at a distance below 1.5σ . An initial set of surface pivots is selected as the most external ions over a mesh of 3×3 prisms, and the initial intrinsic surface is the *minimal area* surface going through these $N_p = 9$ initial pivot ions. Then we incorporate, one by one, new surface pivots at those ions which are closer to the minimal surface, and recalculate the new intrinsic surface $\xi(\mathbf{R}, q_m)$, to go through all the previously selected pivots, until we reach a target occupation of the first layer $n_0 = N_p/A$, which is the essential control parameter in the procedure.¹⁹ As in the case of dielectric liquids, the choice of n_0 is done looking for the best shape of the intrinsic profile (4), averaged over a few thousand configurations of the liquid slab, so that it does not show peculiar shoulders or any other unphysical behavior. We get the best representation of the K and Na intrinsic profiles with $n_0\sigma^2 = 0.9 \pm 0.05$, and with $n_0\sigma^2 = 0.8 \pm 0.05$ for liquid Li. These values of n_0 are higher than $n_0\sigma^2 \approx 0.72$, which was found appropriate for the dielectric simple fluid soft-model,¹⁸ but lower than the value, $n_0\sigma^2 = 1.1$, obtained for water.²⁰ Note also that the lower value for Li is in accordance with the smaller amplitude of the first oscillation in the mean ionic profile as compared with those of Na and K.¹²

The intrinsic profile (4), at the sharpest level $q_u = q_m$, has a delta function term $n_0\delta(z)$ to represent the first liquid layer, followed by a strong layering structure, decaying towards the liquid bulk. The smoother intrinsic profiles, associated to any q_u below q_m , may be obtained by keeping the same Fourier components as in $\xi(\mathbf{R}, q_m)$ for $q < q_u$, but neglecting all those for $q \geq q_u$. Such surface $\xi(\mathbf{R}, q_u)$ follows the longer wavelength fluctuations of the liquid surface, but it does not go exactly through the ions on the first layer. The oscillating structure in $\bar{\rho}(z, q_u)$ becomes gradually damped with decreasing q_u , down to the mean density profile of our simulations, $\rho(z, L_x)$, when q_u is pushed to the lower cutoff $q_l = 2\pi/L_x$. Associated to each intrinsic density profile $\bar{\rho}(z, q_u)$ there is a mean square CW amplitude

$$\Delta(L_x, q_u) = \sum_{q=q_l}^{q_u} \langle |\hat{\xi}_q|^2 \rangle, \quad (6)$$

which represents the square Gaussian width of the surface fluctuations eliminated from $\rho(z, L_x)$. Since the surface $\xi(\mathbf{R}, q_m)$ becomes smooth at atomic scale, the mean square Fourier components for $q \rightarrow q_m$ become negligibly small, and there would be no practical effect if q_m is increased. Therefore $\Delta(L_x, q_m)$ represents the full amplitude of the CW with wavelength below L_x , and $\bar{\rho}(z, q_m)$ is the sharpest intrinsic representation of the liquid surface, when the whole CW spectrum has been eliminated.

Notice that our *maximum* wave vector q_m should not be directly compared with the effective upper cutoff q_u^{eff} used in the classical version of the CWT, to represent the total squared width of the CW fluctuations as

$$\Delta_{\text{CWT}}(L_x, q_u^{\text{eff}}) \equiv \sum_{q=q_l}^{q_u^{\text{eff}}} \frac{1}{A\beta\gamma q^2}, \quad (7)$$

assuming that the mean square amplitude of the intrinsic surface Fourier components is $\langle |\hat{\xi}_q|^2 \rangle = (A\beta\gamma q^2)^{-1}$, with the macroscopic area A , and surface tension γ . Since our CW amplitudes decay much faster than this prediction for q approaching q_m , the total square width $\Delta(L_x, q_m)$ becomes equal to $\Delta_{\text{CWT}}(L_x, q_u^{\text{eff}})$ for an effective cutoff $q_u^{\text{eff}}\sigma = 2 \pm 0.5$, well below our maximum wave vector, $q_m\sigma \approx 1.8\pi \approx 5.66$. The uncertainty in q_u^{eff} comes from the choice of the control parameter n_0 , which has very little effect on $\bar{\rho}(z, q_u)$, but which produces relatively large changes on $\langle |\hat{\xi}_q|^2 \rangle$ for large q . This fact reflects the inherent ambiguity, at atomic resolution, in the definition of the intrinsic surface $\xi(\mathbf{R}, q_m)$ associated to each configuration of the liquid surface. The notion of the *first layer* in a liquid surface, used here to define the intrinsic surface, is clearly a *soft concept*, for which we cannot expect a sharp rule. However, it is also a natural and useful concept since it leads to properties like $\bar{\rho}(z, q_u)$ which are essentially robust with respect to reasonable variations in n_0 , or in any other aspect of $\xi(\mathbf{R}, q_u)$. The fact that $\langle |\hat{\xi}_q|^2 \rangle$ decays faster than the CWT prediction for large q is also a generic property of any sensible choice of $\xi(\mathbf{R}, q_u)$, but the specific way of decay, and hence the effective q -dependent surface tension

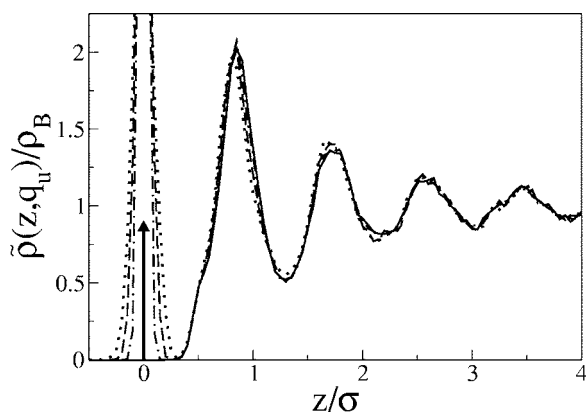


FIG. 2. Ionic intrinsic density profiles of the surface of K. The intrinsic density profiles have been evaluated using an intrinsic surface with an occupation of the first layer $n_0\sigma^2=0.9$, and corrugated up to different values of q_u . Full line and arrow: $q_u=q_m\equiv 9q_l\approx 1.8\pi/\sigma$; dashed-dotted line: $q_u=8q_l\approx 1.6\pi/\sigma$; dashed line: $q_u=7q_l\approx 1.4\pi/\sigma$; and dotted line: $q_u=6q_l\approx 1.2\pi/\sigma$; where $q_l=2\pi/L_x$ is the lower wave-vector cutoff.

$\gamma(q)\equiv(A\beta q^2\langle|\hat{\xi}_q|^2\rangle)^{-1}$, is subject to a relatively large degree of ambiguity.

Before showing the specific results for the intrinsic density profiles we make a technical comment. The average of the mean density profile (3) gives larger statistical noise than the average (4) for the intrinsic profile, using the same number of ionic configurations. In fact in the previous simulation of metallic liquid surfaces¹⁰⁻¹² the mean density profiles were smoothed through the convolution with a narrow Gaussian in order to reduce the statistical noise. The elimination of the long range transverse correlations, generated by the CW fluctuations on the liquid surface, reduce that statistical noise, so that any artificial coarse graining is avoided as unnecessary and inconvenient to keep full account of the sharp resolution in the ionic intrinsic profiles. Besides being a practical advantage, the low statistical noise of the ionic intrinsic density gives support to our method to identify the intrinsic surface, and it confirms that it represents a natural feature of the liquid surface.

The intrinsic profiles with $q_m=1.8\pi/\sigma$ represent the sharpest atomic resolution for the interfacial structures in our computer simulations; the intrinsic surface goes exactly through the center of the pivot atoms, and therefore the intrinsic profile has a delta-function term, $n_0\delta(z)$, to describe the first liquid layer. Using values of q_u below q_m we may give a gradually increasing Gaussian width to this layer, as shown in Fig. 2. The CWT assumption of statistical independence between the intrinsic profile and the intrinsic surface corrugations would predict that all the inner layers of $\tilde{\rho}(z, q_u)$ should have same increase of their square width. However, as reported for simple liquids,^{17,18} such assumption clearly fails for large q_u . The results in Fig. 2 show that the inner structure of the ionic intrinsic profiles is not sensitive to the precise value of the cutoff in the range $q_m\geq q_u\geq 1.4\pi/\sigma$. Only for $q_u=1.2\pi/\sigma$ we start to appreciate a slight decrease in the amplitude of the oscillations further on the first peak. That means that the CWT is not valid in the range

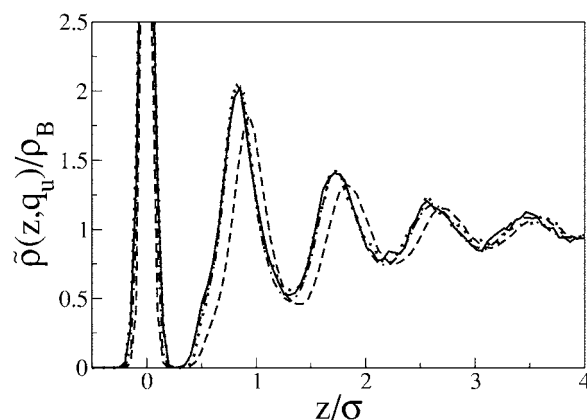


FIG. 3. Ionic intrinsic density profiles, relative to the bulk density, for the three alkali metals K (full line), Na (dotted line), and Li (dashed-dotted line), and for the soft model at $T/T_C=0.12$ (dashed line), using an intrinsic surface corrugated up to $q_u\approx 1.4\pi/\sigma$. The distances z are in units of the position of the first peak of the bulk pair correlation function σ .

$q_u\geq 1.4\pi/\sigma$ of corrugation of the intrinsic surface, and that it may be convenient to use that intrinsic profile to characterize the liquid surface, in a compromise between the sharpness of the representation, and the simplicity of its connection to the mean density profile $\rho(z, L_x)$, through a simple Gaussian convolution.

In Fig. 3 we show the intrinsic profiles $\tilde{\rho}(z, 1.4\pi/\sigma)$ for the three alkali metals, extracted from the *ab initio* computer simulations,¹⁰ and also the results for the simple *soft-alkali* (SA) pair potential model, which was used in the first application of the intrinsic sampling method.^{17,18} As we can see, the qualitative shape of the four intrinsic profiles is very similar, and also similar to the experimental intrinsic profiles of Ga,² and In,³ extracted from x-ray reflectivity data. The four liquids have a compact liquid bulk structure and the propagation of the packing order, from the first peak into the liquid, is very strong. As it was already observed in the analysis of the experimental data^{2,26} and of our previous

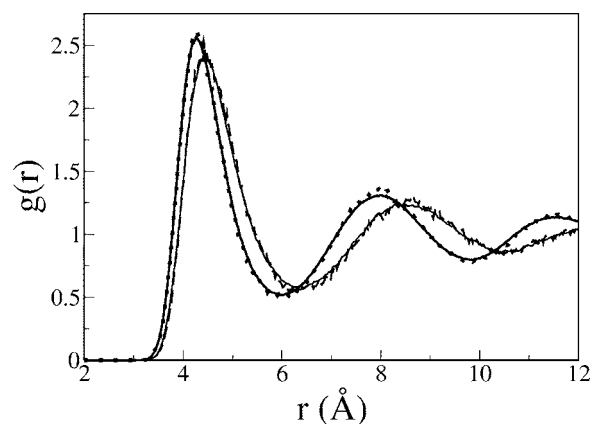


FIG. 4. Pair distributions functions for the surface of liquid K. Dashed line: among ions of the first layer. Thin solid line: averaged over the first slice defined through the mean ionic profile. Dotted line: among ions of the first layer and the other ions. Thick solid line: bulk radial distribution function.

simulations of dielectric isotropic pair model¹⁸ and of water,²⁰ the shape of $\tilde{\rho}(z, q_u)$ for Li, Na, and K is qualitatively similar to that of the pair distribution function $g(r)$ in the bulk liquids, shown in Fig. 4.

On a more quantitative detail, the intrinsic profiles of the three alkali metals are very similar, almost indistinguishable, when represented in terms of their respective atomic diameters. However, the intrinsic profile of the simple pairwise SA model has the positions of the inner peaks clearly displaced to higher values of z . For all the systems the spacing between inner layers is around 0.89σ . However, for the three alkalis there is a contraction of the first interlayer spacing, which becomes 0.83σ , very close to the value of 0.82σ expected for the packing of hard spheres. The SA model, on the other hand, shows an expansion of the first interlayer distance, which is now 0.92σ , representing a relaxation of that distance similar to that observed in the x-ray reflectivity experiments for Ga. Some authors³ claim that in the case of Ga that value is due to the formation of directional bonds that prevent the close packing achieved by the nearly free electron (NFE) metals. In the simple SA model the observed relaxation of the first layer should come from its extremely soft pairwise repulsion, which prevents the close packing.

In the recent *ab initio* molecular dynamics simulations by Gonzalez *et al.*¹⁰⁻¹² of the liquid surface of simple metals, using the same model as here, the authors have studied the variation in the transverse pair correlation function across the interface and they found a surface relaxation produced by a longer nearest neighbor distance for ions in the vicinity of interface than in the bulk. The outermost interfacial region was defined to be a slice (3.1 Å wide in the case of K) comprising the region of z values between the inflection point in the decaying mean ionic density profile and its first minimum. In principle the CW prevent a higher resolution for such an approach, because the projection on z could mix the atoms very close to the surface with those atoms inside the liquid slab. Our operational definition of the intrinsic surface allows a more precise description of the surface correlations because we may select the ions on the intrinsic surface, and those from the inner layers, to obtain separate samplings of their correlation. However, the relatively low rugosity of the liquid K surface gives very similar results with the two methods, as presented in Fig. 4.

The $g(r)$ between the ions on the first layer (the pivots ions) is clearly relaxed with respect to the bulk pair distribution, with a nearest neighbor distance larger (4.46 Å) than the bulk distance (4.26 Å). The correlation between the ions in the first layer and those in the inner liquid is indistinguishable from that of the bulk liquid. Moreover, the nearest neighbor distance does not increase gradually if we take pairs of ions at different depths into the liquid, as soon as one (or the two) ion belongs to the second surface layer, it reaches the bulk nearest neighbor mean distance. This peculiarity of the first liquid layer correlation in metallic systems had not been observed in the dielectric SA model, or in the the SPC/E model of the water, as both exhibit surface radial distribution functions identical to the bulk one.

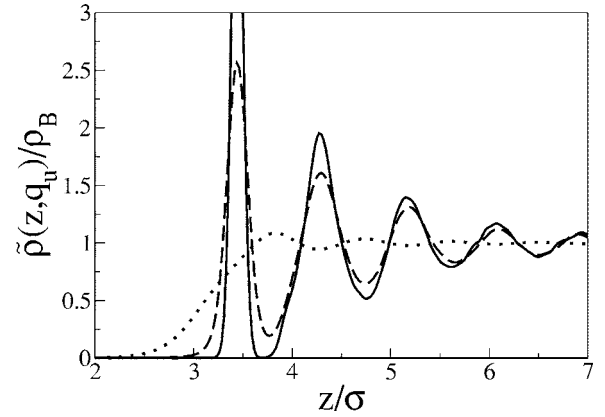


FIG. 5. Ionic (full line), total (core+valence) electron (dashed line), and valence (dotted line) intrinsic density profile $\tilde{\rho}(z, q_u)$ normal to the surface of K, evaluated using an intrinsic surface corrugated up to $q_u \approx 1.4\pi/\sigma$.

IV. K SURFACE STRUCTURE FACTOR AND X-RAY REFLECTIVITY

The aim of this section is the quantitative comparison between our intrinsic sampling in the *ab initio* computer simulations for the surface of liquid K, and the results obtained from the interpretation of x-rays reflectometry experiments in that system. As we commented above, the results of Gonzalez *et al.*¹⁰ offer the first opportunity to check that interpretation, based on the concepts of the CWT, and with an upper cutoff empirically set at $q_u^{\text{eff}} = \pi/\sigma$. The link between the experimental x-ray reflectivity and the electronic intrinsic density profile $\tilde{\rho}(z)$ is established through the intrinsic surface structure factor:

$$\Phi_{\text{elec}}(q_z) = \frac{1}{\rho_{\text{bulk}}} \int dz \frac{\langle d\tilde{\rho}_{\text{elec}}(z) \rangle}{dz} \exp(iq_z z), \quad (8)$$

whose squared modulus $|\Phi_{\text{elec}}(q_z)|^2$ gives the contribution to the differential cross section from the diffuse scattering of the averaged intrinsic density electronic along the surface normal coordinate z , in the absence of the capillary waves⁴ which, according to the CWT, are extracted by multiplying the ratio between the observed and the Fresnel reflectivity by the inverse Gaussian $\exp(\Delta_{\text{CWT}} q_z^2)$, with the effective Gaussian square width in Eq. (7).

We may obtain directly the intrinsic surface structure factor from our simulations, without relying on the CWT assumptions, because the same procedure described in the previous section, to get the ionic intrinsic profiles, may be used to evaluate the electronic intrinsic density profiles at any allowed level of corrugation for the intrinsic surface, and, from that, $|\Phi_{\text{elec}}(q_z, q_u)|^2$. We have obtained very similar results for Li, Na, and K, so that all of the following discussion would be based on the later, for which there are experimental results from x-ray reflectivity.⁴ In Fig. 5 we present the valence and total electronic intrinsic profiles using an intrinsic surface corrugated up to $q_u = 1.4\pi/\sigma$, for comparison we present also the ionic intrinsic profile at the same q_u . The main contribution to the total electron intrinsic profile, $\tilde{\rho}_{\text{elec}}(z, q_u)$, comes from the core electrons, which follow the

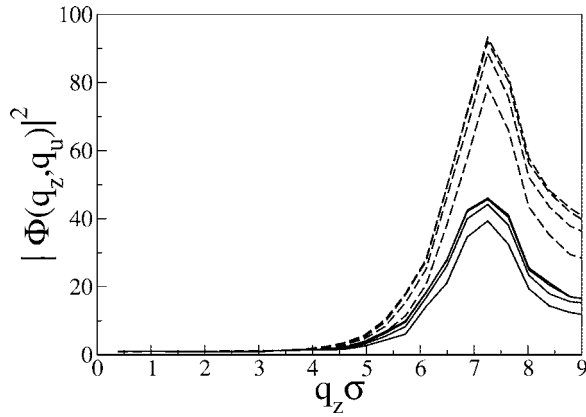


FIG. 6. Surface structure factor $\Phi(z)$ from our simulations of K, using intrinsic surfaces corrugated up several q_u . Full lines: results for the total electron surface structure factor. Dashed lines: results for the ionic surface structure factor. In both cases the different curves with decreasing height of the peak correspond to decreasing wavelength: $q_u = q_m \approx 1.8\pi/\sigma$, $q_u \approx 1.6\pi/\sigma$, $q_u \approx 1.4\pi/\sigma$, and $q_u \approx 1.2\pi/\sigma$.

ionic structure $\tilde{\rho}(z, q_u)$, convoluted with the smooth distribution of core electrons for each ion. That smoothing reduces the sensitivity to the choice of a particular cutoff q_u , with no appreciable changes in the range $q_m \geq q_u \geq 1.4\pi/\sigma$. The contribution from the valence electrons is very delocalized, and it does not change at all in the range $q_m \geq q_u \geq 1.4\pi/\sigma$, or even further down in q_u . Nevertheless, the comparison with the mean profile in Fig. 5 shows that the delocalized valence electrons follow the ions in the CW fluctuations of long wavelength, since their intrinsic sampling gives a clear oscillatory structure, in opposite phase to the ionic oscillations; while in the mean profile in Fig. 1, those oscillations are more strongly damped.

From the total intrinsic electronic profile, we have used Eq. (8) to calculate $|\Phi_{\text{elec}}(q_z, q_u)|^2$, which may be directly compared with the experimental data for liquid K. Also, we may obtain the ionic surface structure factor, $|\Phi_{\text{ion}}|^2$, by inserting in Eq. (8) the ionic intrinsic density profile, instead of total electronic intrinsic density distribution, which is convenient for the comparison with previous results for simple fluid models. Both surface structure factors, $|\Phi_{\text{elec}}|^2$ and $|\Phi_{\text{ion}}|^2$, Fig. 6, have a clear maximum at wave vectors around a peak value $q_z \approx q_{\text{peak}} \approx 2\pi/\sigma$, associated to the atomic layering. The peak is obviously higher for the ionic than for the electronic structure factor because of the weak delocalization of the core electrons, and the stronger one of the valence electrons. However, at $q_z < q_{\text{peak}}/2$ we found that the ionic and the electronic surface structure factors become similar, as shown also in Fig. 7, together with the experimental data for potassium and other cold liquid metals. The experimental data for K are restricted to $q_z \leq 0.8q_{\text{peak}}$, because at larger q_z the signal, damped as $\exp[-\Delta_{\text{CWT}}(L_x, q_u^{\text{eff}})q_z^2]$ by the CW fluctuations, goes below the noise level; the lower damping exponent $\eta = \pi/(\beta\gamma\sigma^2)$ for Ga and In gives experimental access to a longer range of q_z which reaches the maximum observed with the intrinsic sampling of computer simulations for simple fluids. The value of $|\Phi_{\text{elec}}|^2$ at the maximum de-

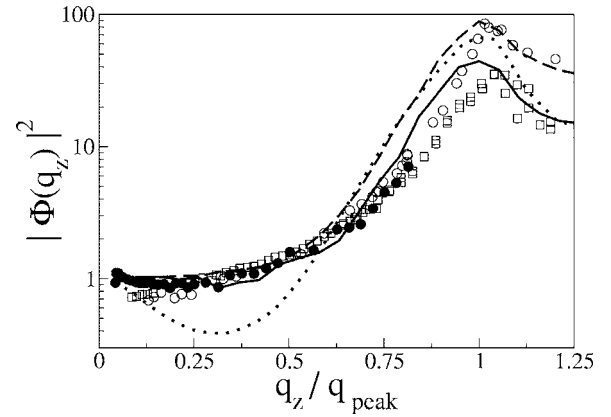


FIG. 7. Surface structure factor $\Phi(z)$ for liquid Ga (open circles), liquid In (open squares), and liquid K (closed circles) obtained from x-ray reflectivity in Ref. 4, as a function of q_z/q_{peak} where q_{peak} is the value of q_z at which the layering peak is either observed or expected. The full line is our total electron $\Phi_{\text{elec}}(z, q_u)$ using the intrinsic surface corrugated up to $q_u \approx 1.4\pi/\sigma$. The dashed line is our ionic surface structure factor of K at the same resolution. Finally the dotted line is the ionic surface structure factor of the soft model at $T/T_C = 0.12$ and $n_0\sigma^2 = 0.72$.

pends on the level of corrugation allowed for intrinsic surface, and it scales as $(q_u^{\text{eff}})^{2\eta}$, with the empirical choice of the effective CWT cutoff, so that the difference between the value $q_u^{\text{eff}}\sigma = \pi$ used by the experimentalists, and our estimation $q_u^{\text{eff}}\sigma \approx 2 \pm 0.5$ for K, would imply a overestimation in the experimental intrinsic $|\Phi_{\text{elec}}|^2$ by a factor of 2 at q_{peak} , and a factor of 1.4 at the largest q_z with experimental data for K. Moreover, the effective mean square CW amplitude $\Delta_{\text{CWT}}(L_x, q_u^{\text{eff}})$ depends on the product $L_x q_u^{\text{eff}}$, so that the empirical choice of q_u^{eff} is merged with the estimation of the effective sampled area $A = L_x^2$, which in fact requires a careful integration over the dispersion angles allowed by the x-ray detectors.²⁹ Altogether, we may say that the comparison between our $\Phi_{\text{elec}}(q_z, q_u)$ and the experimental results should allow for a 50% error bar at the largest experimental q_z , so that we cannot distinguish between different broadenings of the intrinsic profiles similar to those in Fig. 2, and the quantitative agreement observed in Fig. 7 between the experimental data and our results for $\Phi_{\text{elec}}(q_z, q_u)$, without any free parameter, is even better than what could be expected.

At lower q_z the uncertainty produced by the value of $L_x q_u^{\text{eff}}$ decreases rapidly, at $q_z = q_{\text{peak}}/2$ the error bar induced by $L_x q_u^{\text{eff}}$ would be about 15%. This is important because any possible relaxation of the first interlayer spacing shows up in $|\Phi(q_z, q_u)|^2$ for $q_z < q_{\text{peak}}/2$; as shown by the comparison in Fig. 7 with the surface structure factor of the SA model,^{17,18} which has a clear relaxation of that interlayer distance. The minimum of $|\Phi(q_z, q_u)|^2$ for this model at $q_z \approx 0.3q_{\text{peak}}$ is not observed in our present computer simulations, nor in the experimental results for liquid K. That minimum is directly produced by the difference between the intrinsic profiles in Fig. 3, and it can be removed if the first peak in the SA intrinsic profile is shifted to the same interlayer distance as the inner peaks. The reduction of the first layer occupancy n_0 may also generate a minimum in $|\Phi(q_z, q_u)|^2$, and the ob-

served values for the SA model, $n_0\sigma^2 \approx 0.75$, and for the present simulation of K, $n_0\sigma^2 \approx 0.90$, point in the same direction as the interlayer spacing, although the later is clearly the most relevant.

Some authors²⁷ have used the observation of $|\Phi(q_z)|^2$ decreasing from the unity at low q_z as a signature that no surface layering would be present. However, our results show that systems with a strongly oscillatory intrinsic surface structure, as that shown in Fig. 7 for the SA model, may have a fast decay of $\Phi(q_z)$ for $q_z < 0.3q_{\text{peak}}$, followed by a rise at larger q_z , which may, however, be beyond the range of the experimental reflectivity results.

It is clear that the relationship between the intrinsic profiles and the surface structure factor is quite subtle. Different intrinsic profiles may produce essentially identical reflectivity curves,²⁸ while a slight modification of the intrinsic profiles may produce drastic changes in the reflectivity curves, lending some ambiguity to the experimental analysis in order to construct a model density profile and compare its calculated reflectivity to the experiment. Our intrinsic sampling procedure gives direct access to $\tilde{\rho}(z, q_u)$, along computer simulations of model systems, and it provides useful information to explore that relationship.

V. DISCUSSION

The first point to be stressed is that, for free liquid surfaces, any layered density profile either extracted from experimental data, or directly averaged over computer simulations, has to be considered as a function $\rho(z, L_x)$, depending on the sampled transverse area $A \equiv L_x^2$. The waiving of the L_x dependence, often done in the comparison of monotonic density profiles, becomes highly misleading for oscillatory density distributions, since the CW surface fluctuations damp the molecular layering structure with a factor $L_x^{-\eta}$, and the exponent $\eta \approx \pi/(\beta\gamma\sigma^2)$ inverse to the stiffness of the surface; for liquid potassium near its triple point studied here, the value of $\eta \approx 0.73$ is already large enough to produce a strong dependence of $\rho(z, L_x)$ on L_x , and the direct comparison of the results for different sampling sizes becomes meaningless.

In consequence, the interpretation of the results from density functional approximations, or any other theoretical treatment without an explicit dependence on L_x , becomes uncertain for any fluid interface. For typical density functional approximations of simple liquid models the effective sampled length, L_x^{eff} , has been estimated to be in the range of ten molecular diameters,¹⁵ but there is no estimation of L_x^{eff} for the much complex theoretical procedures needed to describe the interaction between ions and free electrons in a liquid metal. The mixed approach, with perturbation theory and computer simulation, developed by Rice and co-workers,¹⁴ treats the electrons in an effective *jellium* distribution, $\rho_{\text{jell}}(z)$, which represents the mean ionic distribution averaged over the transverse (x, y) plane, so that the valence electrons do not have any CW fluctuation. This is reflected in the relatively strong layering observed for the valence electrons in that approach, closer to our intrinsic description in $\tilde{\rho}_{\text{elec}}(z, q_u)$, than to the mean profile $\rho_{\text{elec}}(z, L_x)$.

On the other hand, the ions appear to have transverse fluctuations similar to those observed in our OFAIMD, since the mean ionic profiles are similar to those of Rice *et al.*¹⁴ The CW fluctuations with long wavelength imply local correlated displacements of the ionic and the electronic distributions, and the correct dependence of the mean density profiles with L_x requires a consistent description of these fluctuations for both the ions and the valence electrons. The application of the intrinsic sampling method^{17,18} to the ionic configurations obtained along the computer simulations for liquid metals with that method, for a given $\rho_{\text{jell}}(z)$, could be used to extract their effective CW spectrum, and therefore to provide a calibration of the effective sampled length to be associated to those results. Meanwhile, the results of that theoretical method may be considered relevant only for the *intrinsic* aspects of the density distribution, like the integrated density over the first layer, or the possible relaxation of the first interlayer distance; but not for those aspects of $\rho(z, L_x)$ like the width of the layers, or the amplitude of the density oscillations, which can only be interpreted for a known (effective) transverse size L_x .

The *ab initio*, orbital-free, computer simulations used here, following the method of Gonzalez *et al.*,¹⁰ do not impose any artificial restriction on the fluctuations of the liquid surface, and the CW spectrum extracted with our intrinsic sampling method gives the behavior $|\hat{\xi}_q|^2 \sim q^{-2}$, for q near the lower cutoff $q_l = 2\pi/L_x$, as predicted by the CWT for a free fluid interface, in the absence of any pinning external field. Therefore our mean density profiles $\rho(z, L_x)$ are certainly associated to the transverse sampling size imposed by the simulation box size L_x . The CWT could be easily used “upward” to incorporate all the CW with wavelengths between that L_x and the much larger experimental sampling length, L_x^{exp} , obtained from the careful calibration of the incident beam, and the detectors, in the x-ray reflectometry experiments.²⁹ However, such Gaussian convolution of $\rho(z, L_x)$ would imply a severe loss of information on the structure of the liquid surface, since the layering structure observed in Fig. 1 would fall below the intrinsic noise of the computer simulation in $\rho(z, L_x^{\text{exp}})$.

The increasing accuracy of the x-ray reflectivity data during the last decade has provided enough signal-to-noise ratio as to allow a riskier “downward” use of the CWT, with a Gaussian deconvolution to extract the *intrinsic density profile* $\tilde{\rho}(z, q_u)$, assuming that the macroscopic surface tension may be used to get the effective surface Hamiltonian up to an empirical upper cutoff $q_u = \pi/\sigma$. The comparison between the experimental results for liquid potassium and the present analysis of the intrinsic surface properties in a realistic computer simulation of the same liquid metal provides the first opportunity for a quantitative test on that interpretation. As expected on physical grounds, and observed in previous applications of the intrinsic sampling method to simple liquids,^{17,18} at wavelengths approaching the molecular size, the CW spectrum depends on the specific definition of the intrinsic surface associated to each molecular configuration. Within the method used here, we observe clear differences between the values of the mean squared amplitude, $\langle |\hat{\xi}_q|^2 \rangle$, for $\pi < q\sigma < 2\pi$, obtained within the range of acceptable val-

ues for the two-dimensional density of the *first liquid layer*, which is self-consistently defined as the locus of the intrinsic surface. Nevertheless, any sensible choice leads to smooth decays of the corrugations, which for $q = \pi/\sigma$ are already well below the classical CWT assumption, $\langle |\hat{\xi}_q|^2 \rangle_{CWT} = (A\beta\gamma q^2)^{-1}$; and they vanish as q approaches our maximum $q_m = 1.8\pi/\sigma$. The effective CWT upper cutoff, empirically taken at $q_u^{\text{eff}} = \pi/\sigma$ in the interpretation of the x-ray reflectivity data, overestimates our result $q_u^{\text{eff}}\sigma = 2 \pm 0.5$, for the effective upper cutoff which would give the same Gaussian width $\Delta_{CWT}(L_x, q_u^{\text{eff}})$ as that observed in our larger wave-vector range ($2\pi/L_x \leq q < q_m$), but with the mean square CW amplitude $\langle |\hat{\xi}_q|^2 \rangle$ falling below the classical CWT prediction $1/(\beta\gamma A q^2)$ for large q . That overestimation of q_u^{eff} would produce a factor $(\pi/2)^{2\eta} \approx 2. \pm 0.6$, at the peak value of the surface structure factor in Fig. 7, and a much weaker correction over the lower range of q values for which there are experimental data. Such corrections would be of little relevance for the interpretation of the available results for K (over the logarithmic scale in Fig. 7), although they should be taken into account when experimental data for larger q become available, as they already are for Ga and Hg, allowing a more detailed analysis.

Without any adjustable parameter, the surface structure factor from our electronic density profiles follows remarkably close to the experimental data for the liquid K surface in Fig. 7. Notice that the electronic profiles are smoother than the ionic ones, the differences in the surface structure factor, $\Phi_{\text{elec}}(q_z, q_u)$, within intrinsic samplings in the range $1.8 \leq q_u\sigma < 1.2$, are well below the possible resolution in the comparison with the experimental data, so that all the ionic intrinsic profiles presented in Fig. 2 would be compatible with the experimental data. In fact, the reduced range of q of the experimental data leave a wider uncertainty for the possible ionic structures compatible with the observed values of the electronic structure factor, and we cannot expect to discern between the direct Gaussian convolution of $\tilde{\rho}(x, q_u)$ to get $\rho(z, L_x)$ assumed by the CWT, and the more complex relationship observed in simple liquid surfaces for $q_u\sigma > 1$. However, there is an aspect of the intrinsic density profiles observed in our computer simulations which may be directly compared with the available experimental data, this is the lack of a clear minimum in $\Phi_{\text{elec}}(q_z, q_u)$, at $q_z < q_{\text{peak}}$, which had been observed in computer simulations of the simple pairwise model interaction SA.^{7,8} The high resolution of our intrinsic density profiles allows the clear identification of that minimum as a consequence of the relaxation in the first interlayer density in the SA model, which does not appear in the present realistic simulations of the alkali metals.

Altogether, we may say that within the available experimental data, there is a very good agreement between the predictions of the orbital-free *ab initio* computer simulation results²¹ and the x-ray reflectometry on the surface of liquid potassium.⁴ Such comparison is taken to its sharper level by the application of the intrinsic surface sampling method,¹⁷⁻¹⁹ which had been developed and previously used for computer simulations of simple liquids. A very recent application to the water surface,²⁰ and the present work for NFE liquid metals, Li, Na, and K, proves that it is a powerful tool to

study the inherent structure of the surface without the burring effect of thermal capillary waves, which may be important even at the reduced transverse dimensions of a typical liquid slab simulation.

The application of the method to simple fluid models (LJ, SA,...) had proved that the strong layering structure observed in the experimental x-ray reflectivity data for the very cold liquid metals (Ga, In, and Hg), were a typical property of any intrinsic density profile for liquid surfaces, rather than a peculiarity of liquid metals. Again we find here that the ionic intrinsic profiles of the liquid alkali metals show as strong layering structure, with a decay towards the inner liquid similar to that of the oscillations in the bulk liquid pair distribution function, produced by the compact packing structure of the system. The qualitatively different aspects of these liquid surfaces in the mean density profiles $\rho(z, L_x)$ reflect mainly the different CW damping of the layering $\sim L_x^{-\eta}$, with η ranging from below 0.5 for the cold liquid metals, to 0.73 for potassium, and 2.31 for LJ at its triple point. Despite their qualitative similarity, the intrinsic profiles of different systems showed interesting differences in the intrinsic aspects of the layering structure, the density of the first liquid layer, self-consistently defined with the intrinsic sampling method, as the number of surface pivots per unit area, $n_0 = N_p/A$, is $n_0\sigma^2 = 0.9 \pm 0.05$ for K and Na, and $n_0\sigma^2 = 0.8 \pm 0.05$ for Li, higher than the value, $n_0\sigma^2 \approx 0.72$, obtained for the dielectric SA simple fluid model,¹⁸ and lower than the value $n_0\sigma^2 = 1.1$ for water.²⁰ The first interlayer spacing in the three alkali liquid metals is found to be 0.83 times the bulk nearest neighbor distance, very close to the ratio 0.82 for the packing of hard spheres; this is consistent with the NFE character of these liquid metals, without any tendency to form directional bonds. The experimental results for In give similar close-packing interlayering distance, while for liquid Ga the first interlayer distances appear to be relaxed to a ratio 0.92, probably because of the directional bonds between *d*-orbitals. The same ratio is observed in the intrinsic profiles from Monte Carlo simulation of the pairwise SA model, which was constructed^{7,8} to reproduce the low ratio between the triple and the critical temperatures characteristic of the above liquid metals. This effect was achieved by an artificially soft core repulsion, over an original model which would reproduce the energy of expanded alkali solids, and the observed first layer relaxation is most probably the result of that ultrasoft repulsive core. The surface relaxation in our intrinsic profiles is confined to the first interlayer spacing, without any appreciable change for the ions in the inner layers.

All these intrinsic surface properties are revealing a sharp view of liquid interfaces, which may be extracted with the intrinsic sampling method in computer simulations for model systems. The first contact with experimental data has been established for the surface of liquid potassium; and we may hope for the near future application to the colder liquid metals, for which the experimental data are much more accurate, although they would require a more complex theoretical treatment of the electron-ion interactions. From the experimental side, the thermally excited capillary waves prevent

the observation of the specular reflection peak for values of q_z larger than 1.6 \AA^{-1} for liquid K. Any increase of the x-ray reflectivity resolution would also provide very valuable experimental data, at higher q_z , which could be compared with our present results. Finally, there are other intrinsic aspects of the liquid K surface extracted from our computer simulations, which would be very interesting to compare with experimental observations; like the surface relaxation of the pair distribution, or the intrinsic profile of the delocalized valence electrons, which oscillates out of phase with the

(much larger) contribution from the core electrons tightly associated to the ions.

ACKNOWLEDGMENTS

This work has been supported by the Dirección General de Investigación, Ministerio de Ciencia y Tecnología of Spain, under Grants No. FIS2004-05035-C03 and MAT2005-03415, the Comunidad Autónoma de Madrid under Grant No. S-0505/ESP-0299, and the EU FEDER program.

-
- ¹O.M. Magnussen, B.M. Ocko, M.J. Regan, K. Penanen, P.S. Pershan, and M. Deutsch, *Phys. Rev. Lett.* **74**, 4444 (1995); E. DiMasi, H. Tostmann, B.M. Ocko, P.S. Pershan, and M. Deutsch, *Phys. Rev. B* **58**, R13419 (1998).
- ²M.J. Regan, E.H. Kawamoto, S. Lee, P.S. Pershan, N. Maskil, M. Deutsch, O.M. Magnussen, B.M. Ocko, and L.E. Berman, *Phys. Rev. Lett.* **75**, 2498 (1995).
- ³H. Tostmann, E. DiMasi, P.S. Pershan, B.M. Ocko, O.G. Shpyrko, and M. Deutsch, *Phys. Rev. B* **59**, 783 (1999).
- ⁴O. Shpyrko, P. Huber, A. Grigoriev, P. Pershan, B. Ocko, H. Tostmann, and M. Deutsch, *Phys. Rev. B* **67**, 115405 (2003).
- ⁵H. Tostmann, E. DiMasi, O.G. Shpyrko, P.S. Pershan, B.M. Ocko, and M. Deutsch, *J. Phys. Chem.* **102**, 1136 (1998).
- ⁶H. Mo, G. Evmenenko, S. Kewalramani, K. Kim, S.N. Ehrlich, and P. Dutta, *Phys. Rev. Lett.* **96**, 096107 (2006).
- ⁷E. Chacón, M. Reinaldo-Falagán, E. Velasco, and P. Tarazona, *Phys. Rev. Lett.* **87**, 166101 (2001).
- ⁸E. Velasco, P. Tarazona, M. Reinaldo-Falagán, and E. Chacón, *J. Chem. Phys.* **117**, 10777 (2002).
- ⁹D. Li and S.A. Rice, *J. Phys. Chem. B* **108**, 19640 (2004).
- ¹⁰D.J. González, L.E. González, and M.J. Stott, *Phys. Rev. Lett.* **92**, 085501 (2004).
- ¹¹L.E. González, D.J. González, and M.J. Stott, *J. Chem. Phys.* **123**, 201101 (2005).
- ¹²D.J. González, L.E. González, and M.J. Stott, *Phys. Rev. B* **74**, 014207 (1996).
- ¹³M.A. Gómez and E. Chacón, *Phys. Rev. B* **46**, 723 (1992); **49**, 11405 (1994).
- ¹⁴J. Harris, J. Gryko, and S. Rice, *J. Chem. Phys.* **87**, 3069 (1987); D. Chekmarev, M. Zhao, and S. Rice, *ibid.* **109**, 768 (1998).
- ¹⁵R. Checa, E. Chacón, and P. Tarazona, *Phys. Rev. E* **70**, 061601 (2004).
- ¹⁶F.P. Buff, R.A. Lovett, and F.H. Stinger, *Phys. Rev. Lett.* **15**, 621 (1965).
- ¹⁷E. Chacón and P. Tarazona, *Phys. Rev. Lett.* **91**, 166103 (2003).
- ¹⁸P. Tarazona and E. Chacón, *Phys. Rev. B* **70**, 235407 (2004).
- ¹⁹E. Chacón and P. Tarazona, *J. Phys.: Condens. Matter* **17**, S3493 (2005).
- ²⁰E. Chacón, P. Tarazona, and J. Alejandre, *J. Chem. Phys.* **125**, 014709 (2006).
- ²¹D.J. González, L.E. González, J.M. Lopez, and M.J. Stott, *Phys. Rev. B* **65**, 184201 (2002); *J. Non-Cryst. Solids* **312–314**, 110 (2002).
- ²²P. Hohenberg and W. Kohn, *Phys. Rev.* **136**, A864 (1964); also W. Kohn and P. Hohenberg, *ibid.* **140**, A1133 (1965).
- ²³B.G. Walker, C. Molteni, and N. Marzari, *J. Phys.: Condens. Matter* **16**, S2575 (2004); **18**, L269 (2006).
- ²⁴J.A. Alonso and L.A. Girifalco, *Phys. Rev. B* **17**, 3735 (1978); E. Chacón, J.E. Alvarellos, and P. Tarazona, *ibid.* **32**, 7868 (1985); Y.A. Wang and E.A. Carter, in *Theoretical Methods in Condensed Phase Chemistry*, edited by S.D. Schwartz (Springer, New York, 2002), pp. 117–184.
- ²⁵P. García-González, J.E. Alvarellos, and E. Chacón, *Phys. Rev. B* **53**, 9509 (1996).
- ²⁶P.S. Pershan, *Colloids Surf.*, **A** **171**, 149 (2000).
- ²⁷O. Shpyrko, M. Fukuto, P. Pershan, B. Ocko, I. Kuzmenko, T. Gog, and M. Deutsch, *Phys. Rev. B* **69**, 245423 (2004).
- ²⁸E. DiMasi, H. Tostmann, B.M. Ocko, P.S. Pershan, and M. Deutsch, *J. Phys. Chem. B* **103**, 9952 (1999).
- ²⁹A. Braslau, P.S. Pershan, G. Swislow, B.M. Ocko, and J. Als-Nielsen, *Phys. Rev. A* **38**, 2457 (1988).